ETH
Eidgenössische Technische Hochschule Zürich
Swiss Federal Institute of Technology Zurich

Lead Coupling Effects in Double Quantum Dots

Semester Thesis in the group of Prof. Dr. A. Wallraff
QUDEV, ETHZ

Natascha S. Hedrich

Tuesday 8th December, 2015

Advisors: Anna Stockklauser
Department of Physics, ETH Zürich

Contents

Chapter 1

Introduction

In recent years, the application of microwave measurement techniques to quantum dots has opened up new avenues for transport measurements [1, 2]. The use of microwave resonators in superconducting circuits is important in quantum information processing. These resonators can be coupled to qubits, allowing for qubit preparation, manipulation and readout [3]. In particular, we can couple the resonator to a quantum dot.

A quantum dot is a semiconductor nanostructure, providing a confining potential for electrons in three dimensions. Quantum dots (QDs) have proven to be an ideal tool for studying single electron transport [4]. Sometimes called "artificial atoms", QDs have well defined energy levels due to the strong confinement. They can be formed in several ways, including self-assembly due to lattice mismatch in the semiconductor materials, or through metallic gates deposited on the surface of a semiconductor heterostructure. The latter is the form of quantum dot that will be the focus of the discussion. Furthermore, we can couple two quantum dots to form a double quantum dot (DQD). There have been proposals for using such DQDs in quantum information to realize various critical components, such as a CNOT gate [5, 6]. As with single QDs, a property of interest in DQDs is the single electron transport. The electrons must tunnel through potential barriers formed between two gates in order to move from the source to drain. In particular circumstances, in doing so, the electrons will emit a photon. These photons, when emitted into the resonator, can be measured allowing us to obtain more information about the electron transport.

As with all quantum systems, DQDs suffer from decoherence, meaning that the energy levels within the dots are broadened. However, this broadening can also be due to coupling to the source and drain [7, 8]. In the following discussion, we want to examine more closely the effect of this coupling on both the quantum state broadening as well as the dephasing, that is, the rate at which we lose information about the phase of our system. We will

begin in Section 2 by discussing DQDs in more detail. We will examine the structure, the various forms of transport and finally, the broadening of the energy levels. In Section 3, we will discuss the experimental setup and how we ensured well-defined coupled quantum dots. We will then continue by describing the various detection methods in Section 4. Three measurement techniques are of particular interest as they allow us to extract important transport parameters - the lever arm, inter-dot tunnel coupling and emission linewidth. Finally, in Section 5, we discuss our results and show the relationship between the coupling to source and drain and the dephasing as well as quantum dot broadening.

Chapter 2

Coupled Quantum Dots

Quantum dots are very useful tools in studying single-electron transport [4]. These semiconductor nanostructures can be manufactured using varying methods, but those of interest in this discussion are DQDs, having a form similar to that shown in Figure 2.1. Metallic gates are deposited on a

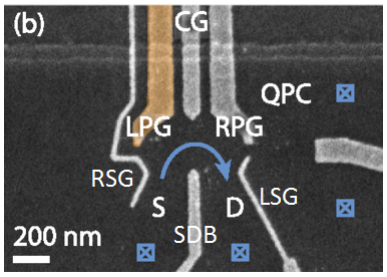

Figure 2.1: Scanning electron micrograph of the gate-defined quantum dot used in the remainder of the study. Here, the DQD is formed using the 6 gates to the left (RSG, LPG, CG, RPG, LSG and SDB clockwise from left). The QPC gate allows us to determine the number of electrons in the quantum dot, but is not required in the experiments discussed here. This image is modified from [9]

semiconductor, most often a GaAs/AlGaAs heterostructure, with an embedded 2D electron gas. By applying negative voltages to the gates, the 2DEG below the gate is depleted, leading to a pinching of the electron flow in the 2DEG between two gates. To form these DQDs, we need 6 gates - two side gates (RSG and LSG), two plunger gates (LPG and RPG) a center gate (CG) and a source-drain barrier (SDB). Note that we also have a quantum point contact (QPC), which is shown in Figure 2.1. However, we will ignore it for our discussion, as we do not need it. The left QD is defined by the LSG, LPG, CG and SDB and similarly for the right QD. The RSG and LSG along with the SDB control the tunnel coupling rate to the drain and source respectively. Furthermore, CG, and to a lesser extent, SDB control the tunnel

coupling between the two dots. In order to better understand what is meant by the tunnel coupling, we can represent the DQD as two potential wells with source and drain as a continuum of states up to a finite chemical potential μ_S and μ_D respectively as shown in Figure 2.2. The difference between

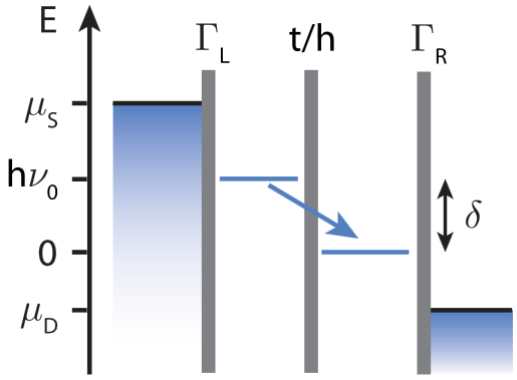

Figure 2.2: A schematic showing the coupled, or double quantum dot (DQD) as two potential wells. The source and drain chemical potentials are given by μ_S and μ_D respectively, the dot levels by μ_1 and μ_2 and the detuning between the dot levels by δ. The tunnel couplings are given by Γ_L, Γ_R and t/h for the left lead, right lead and inter-dot couplings respectively. This figure has been modified from [9].

these chemical potentials is given by the applied bias voltage V_{bias}. Furthermore, the difference between the energy levels within the dots is given by δ, the detuning. Due to the three dimensional confinement, there are discrete energy levels in the two potential wells [4]. These levels can be occupied by electrons, and adjusted by varying the voltages on the plunger gates for the right or left dot. Electrons must then tunnel through all three potential barriers in order to pass from source to drain. The tunnel coupling (both to the leads, Γ_L and Γ_R and the inter-dot coupling rate t/h) then determines the rate at which electrons can tunnel through the barriers.

One very important characteristic of QD transport is Coulomb blockade. This is the process in which tunnelling into a QD state is prevented due to Coulomb repulsion from electrons already occupying the QD. Another electron can only enter the QD if enough energy is supplied to overcome the Coulomb repulsion. This energy is known as the charging energy. In the regime where the bias voltage is much smaller than the charging energy, we would expect to have only single electron transport as there would be no additional states available to the electron.

Now let us consider transport in two configurations; the first being zero bias. In double quantum dots at zero bias, transport is only allowed at particular points known as triple points. This configuration is shown in Figure 2.3. Note that in the stability diagram, the lines form hexagons, which is typi-

cal of DQDs [10]. At these points, all of the energy levels are degenerate,

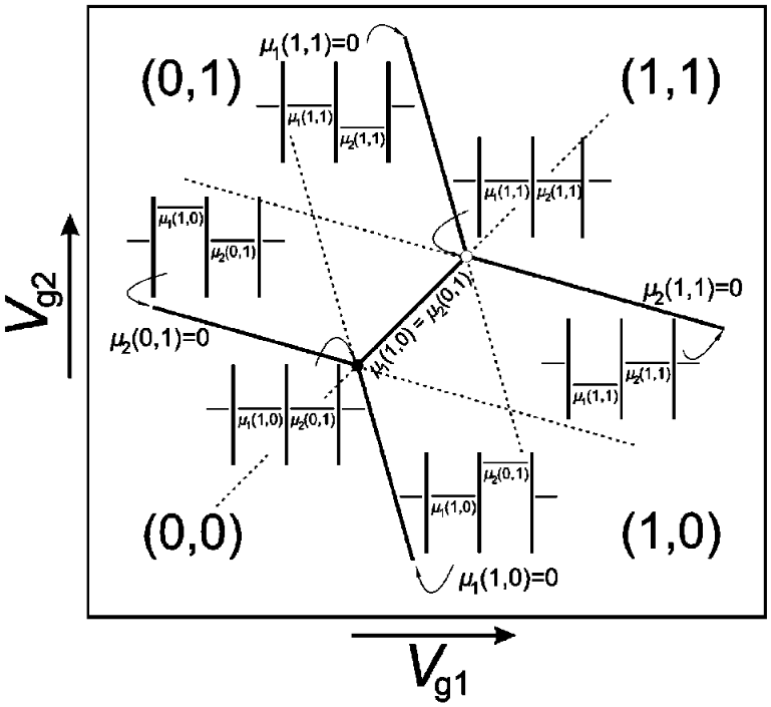

Figure 2.3: In this schematic, we increase V_{g1} (V_{LPG}) and V_{g2} (V_{RPG}) in the direction of the arrows. In doing so, we vary the energy levels of the two dots. Note that we only expect to have transport when all energy levels are degenerate, which only occurs at the two points denoted by the black and white circles (electron and hole transport respectively). The notation used here, $\mu_1(n,m)$, refers to the energy required to add the nth electron to the left dot with m electrons in the right dot and vice versa for μ_2. This figure is taken from [10].

allowing an electron to tunnel through both QDs. There are two kinds of triple points, which are differentiated by the transport direction. We denote a state with N_1 electrons in the first dot and N_2 electrons in the second dot as follows: (N_1, N_2). In this way, the triple points correspond to either hole transport

$$(N_1+1, N_2+1) \rightarrow (N_1+1, N_2) \rightarrow (N_1, N_2+1) \rightarrow (N_1+1, N_2+1),$$

or conversely electron transport

$$(N_1, N_2) \rightarrow (N_1+1, N_2) \rightarrow (N_1, N_2+1) \rightarrow (N_1, N_2)$$

processes [10].

If we then consider the second situation, at finite bias, instead of two transport points, we find two triangular transport regions, also known as finite-bias triangles (FBTs) as shown in Figure 2.4. Applying bias shifts the source

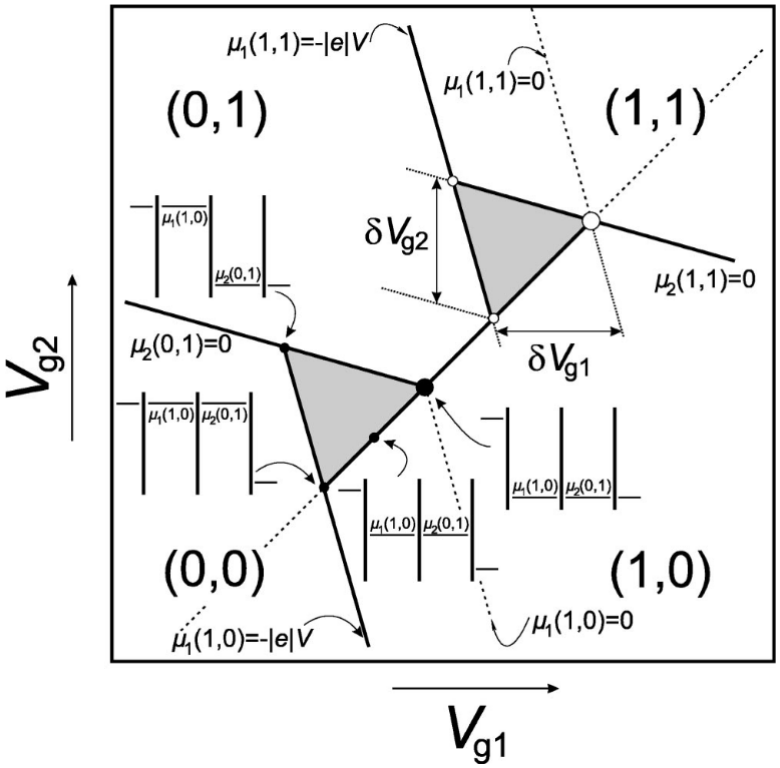

Figure 2.4: A schematic similar to Figure 2.3, but with a finite bias applied. In this case, transport occurs as long as the dot levels sit within the bias window. Thus we obtain triangular transport regions. This diagram is taken from [10].

and drain levels, opening up a bias window. In order to ensure that we only have one available state per dot, we choose a bias voltage that is much smaller than the charging energy. When the electron states in both dots sit within this bias window, transport can occur. Thus, the boundary conditions can be written as follows:

$$-|e|V = \mu_1(1,0), \qquad \mu_1 = \mu_2 \quad \text{and} \quad \mu_2(0,1) = \mu_R = 0,$$

[10] where μ_L, μ_1, μ_2 and μ_R are the chemical potentials of the left lead, left dot, right dot and right lead respectively.

There are several ways now in which electrons can tunnel from one lead to the other, two of which are shown in Figure 2.5. The first which we'll consider is elastic transport, in which the two energy levels in the dots are

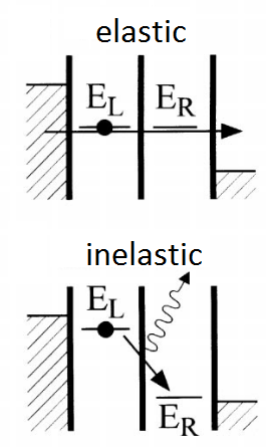

Figure 2.5: Schematic representations of two modes of transport in DQDs. When the dot levels are degenerate, the electron can tunnel elastically from source to drain. When the detuning is non-zero however, the electron must either absorb or emit a particle; often, a photon. This diagram is taken from [12].

degenerate. In this form of transport we can only have current along the bottom side of the triangle where the detuning is zero. Nonetheless, one still finds transport within the entire triangle due to non-resonant processes such as inelastic tunnelling. Due to interactions between the dots and the environment, the electron may absorb or emit a particle such as a phonon or photon and tunnel from source to drain [11, 12]. We are interested in the case where the electron emits a photon. In this case, the current is accompanied by the emission of photons with energies proportional to the detuning between the two dots. It is clear that for positive detuning, where the left dot energy level is higher than that in the right, we should expect an emission signal. However, we see a signal not only for positive, or forward, detuning, but also for negative, or reverse, detuning. This is due to the hybridization of the states in the two quantum dots as shown in Figure 2.6 [9].

Due to the inter-dot tunnel coupling, the left and right dot states hybridize, leading to an energy splitting. This energy splitting can be seen easily by considering a general Hamiltonian H_o and adding a tunnel coupling T.

Let $|\phi_1\rangle$ and $|\phi_2\rangle$ be eigenvectors of the Hamiltonian H_o with energies E_1 and E_2. Now suppose we introduce a tunnel coupling in the form of an off-diagonal matrix [10]:

$$\mathrm{T} = \begin{bmatrix} 0 & t_{12} \\ t_{21} & 0 \end{bmatrix}.$$

The new eigenvalues will then be a superposition:

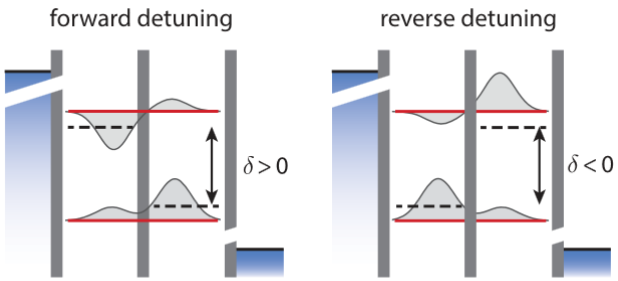

Figure 2.6: A schematic of the forward and reverse detuning cases. In forward detuning, the electron tunnels from the higher left level to the lower right level by emitting, for example, a photon. In the reverse detuning, due to the hybridization, there is still a finite excited state population in the left dot, allowing for the electron to tunnel by emitting a photon. The diagram is adapted from [9].

$$|\Psi_A\rangle = \alpha\,|\phi_1\rangle + \beta\,|\phi_2\rangle$$
$$|\Psi_B\rangle = \tilde{\alpha}\,|\phi_1\rangle + \tilde{\beta}\,|\phi_2\rangle$$

If we now calculate the new eigenenergies, we will need to diagonalize a matrix of the form

$$\begin{bmatrix} E_A - E_1 & t_{12} \\ t_{21} & E_A - E_2 \end{bmatrix},$$

and similarly for E_B. In this way, we obtain the energies of the hybridized states:

$$E_{B,A} = \frac{E_1 + E_2}{2} \pm \sqrt{\frac{1}{4}(E_1 - E_2)^2 + |t_{12}|^2}. \tag{2.1}$$

The hybridization then leads further to a non-zero excited state population in both dots. We can consider two hybridized states $|e\rangle$ and $|g\rangle$ corresponding to a system with an extra electron in the anti-bonding and bonding states respectively. These states can be written as

$$|e\rangle = \cos(\frac{\theta}{2})\,|L\rangle + \sin(\frac{\theta}{2})\,|R\rangle \tag{2.2}$$

and

$$|g\rangle = \sin(\frac{\theta}{2})\,|L\rangle + \cos(\frac{\theta}{2})\,|R\rangle \tag{2.3}$$

where θ is given by $\tan\theta = \frac{2t}{\delta}$ and $|L\rangle$ and $|R\rangle$ are the left and right dot states respectively [9]. Thus, there is a probability, $\alpha = \cos^2(\theta/2)$, of the electron entering the left dot and tunnelling into the right dot by emitting a photon. However, the signal that we see should be much smaller due to the reduced probability. It is from this emission signal that we will later obtain the broadening of the quantum states within the dots.

If we want to measure the emission signal, we need to find a way to detect the emitted photons. This is best done if we couple the DQD to a resonator. In this way, the DQD emits into the resonator when the quantum dot transition is resonant with the resonator frequency, allowing us to collect and measure these photons. However, we need to note that we do not actually have infinitely sharp quantum states but rather, they are broadened. This means that we do not only see a signal when our quantum dot transition is resonant with the resonator, but also within a finite range of frequencies around resonance condition. If we assume Lorentzian broadening of the bare levels, we find the emission power resulting from the hybridized states to be the convolution of the two states and has the form:

$$P(\delta/h) = A(\delta)\frac{\Gamma/2}{(\nu_q(\delta) - \nu_o)^2 + (\Gamma/2)^2}, \tag{2.4}$$

where $A(\delta)$ depends on the excited state population, ν_q is the hybridized transition frequency and ν_o the resonator frequency [7]. The situation is shown graphically in Figure 2.7.

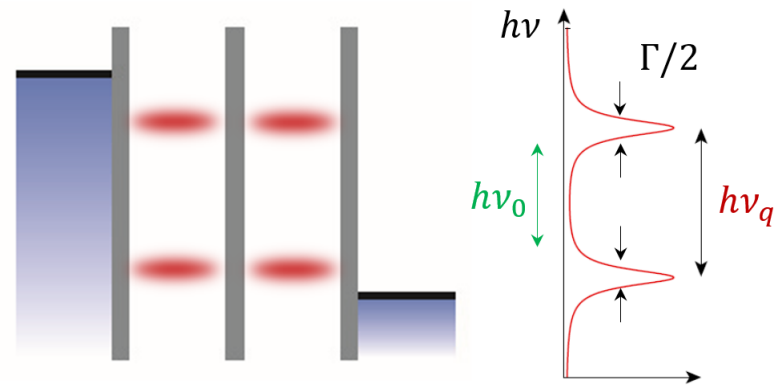

Figure 2.7: Here we see a graphical representation of the broadening of the hybridized states in the DQD on the left. If we assume Lorentzian broadening with a FWHM of $\Gamma/2$ as on the right, we expect to see emission even away from resonance, that is, where $\nu_q \neq \nu_o$. The schematic is taken from [13].

There are several reasons for this broadening to occur. One contribution is charge decoherence (γ), that is, fluctuations in the surrounding 2DEG and

potential background [8]. Another contribution, and that which we chose to focus on, is the coupling to the leads (determined by Γ_L and Γ_R). The goal of the remainder of this semester thesis is to explore the impact the lead coupling has on the level broadening as well as the dephasing (γ_ϕ) of our system; the rate at which we lose phase information. To do so, we will first need to examine the experimental setup and measurement techniques in more detail.

Chapter 3

Setup

3.1 Experimental Setup

In this experiment, we performed our measurements on a gate-defined quantum dot shown in Figure 2.1, whose gates are deposited on top of a GaAs/AlGaAs heterostructure. The heterostructure leads to a 2DEG, which sits approximately 90 nm below the surface and which can be depleted by applying negative voltages to the gates as discussed in previous section. The DQD is then coupled to a 200-nm-thick Al coplanar waveguide resonator as shown in Figure 3.1. This coupling allows us to measure the emission signal as the microwave photons resulting from inelastic tunnelling processes can be emitted into the resonator. The physical coupling is achieved by extending the center conductor of the resonator to form the LPG. The resonator has a bare resonance frequency of $\nu_o = 6.952$ GHz, which determines the frequency at which we can measure an emission signal. The setup sits within a dilution refrigerator at approximately 20 mK.

There are several possibilities for measuring a signal in this setup. The first is to measure the current between source and drain directly (DC). We also have an RF signal ν_r which we can apply to the resonator. By mixing the signal from the resonator with a local oscillator, we can use a heterodyne detection scheme to measure the two quadratures, thereby obtaining amplitude and phase of the signal. This can be seen from the following expression:

$$Ae^{i\phi} = I + iQ \tag{3.1}$$

The third possibility is to measure photons emitted from the DQD into the resonator directly. In this case, the signal is very small, and so we amplify it using a quantum-limited Josephson parametric amplifier (JPA) and high electron mobility transistor (HEMT).

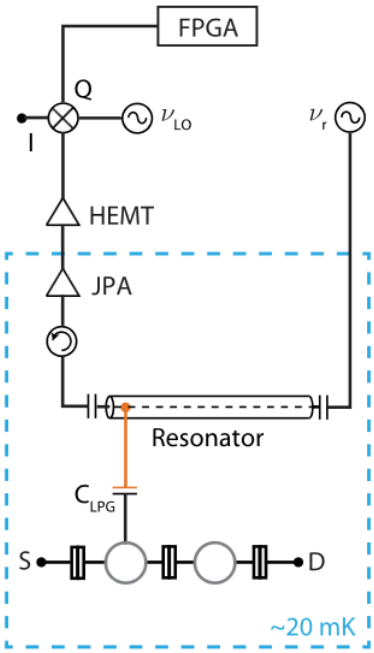

Figure 3.1: A circuit-style diagram showing the DQD, resonator and measurement equipment used in the experiments described in this thesis. The DQD, coupled capacitively via C_{LPG} to the resonator, along with the Josephson parametric amplifier (JPA) sit within a dilution refrigerator at approximately 20 mK. The signal is then further amplified using a HEMT, detected using a heterodyne scheme and processed using a field-programmable gate array (FPGA). An additional RF microwave signal (ν_r) can also be applied to the resonator. The diagram is taken from [9].

3.2 Dot Formation

Before being able to perform transport measurements, one must make sure that the system actually forms two well-coupled quantum dots. This is best determined through DC measurements. As mentioned in Section 2, a DQD has a stability diagram that looks hexagonal. A single quantum dot on the other hand, will exhibit regions of stability that form parallel lines when plotting the LPG and RPG voltages against each other. It is this graphical hint that we can us to tune the DQD.

By adjusting the RSG and LSG, we are able to pinch off one side of either quantum dot, and by adjusting SDB and CG, one can manipulate the side shared between the two dots. For a given configuration, we can scan LPG and RPG, thereby allowing us to see the transition between the single dot and double dot regimes, as shown in Figure 3.2. As these measurements are done at finite bias, we choose a set of FBTs that indicate a nearly symmetric double dot. Due to a strange configuration of the RSG, we have a slight asymmetry, as indicated by the brighter transport regions on one side of the hexagon. This asymmetry can also be seen in the RF measurements. By

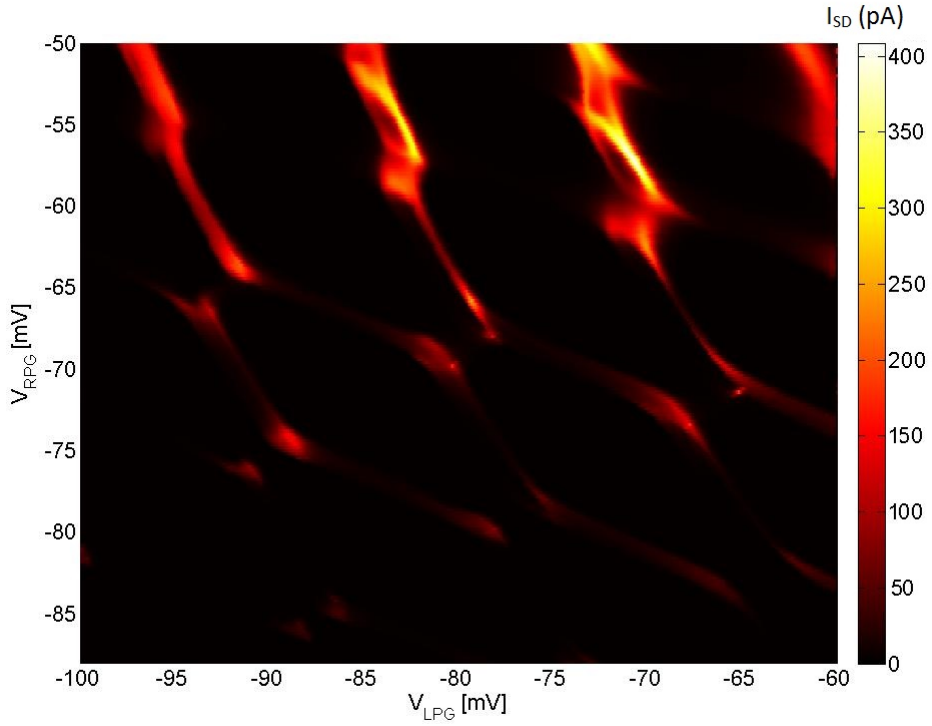

Figure 3.2: Here we see a measured stability diagram of the DQD. The current was measured while varying V_{RPG} and V_{LPG} at a finite bias. One can clearly see that near the top right (small V_{LPG} and V_{RPG}, we find rather straight lines, indicating one large dot. Towards the center, we see nice hexagons form. However, the regime we are interested in is the bottom left, where we can see the individual FBTs.

adjusting RSG, we are able to achieve a symmetric double dot.

Chapter 4

Measurement of Experimental Parameters

Having understood the various methods of electron transport in double quantum dots, it is important to be able to extract the descriptive parameters from measurements. In terms of transport parameters, those of particular interest are the lever arm values (α_R and α_L), the inter-dot coupling (t) and the emission resonance linewidth (Γ).

We chose to perform a series of measurements in which we changed the coupling to the leads while keeping the inter-dot tunnel coupling constant. This way, we could attribute any change in our system to the varying lead coupling.

To determine which voltages to use for a measurement series, we found one configuration in which the DQD seemed to be symmetric (V_{SDB}= -85.5 mV, V_{RSG} = -11.0 mV). We then increased V_{SDB} by 2mV, and adjusted V_{RSG} until the dot was once again symmetric, leading us to V_{RSG} = -14.0 mV. This gave us an idea of how to vary the values of V_{SDB} and V_{RSG} in order to ensure symmetric dots. Between successive steps of our measurement series, we thus varied V_{SDB} by a multiple of 0.2 mV and V_{RSG} by a multiple of 0.3 mV. The other LSG was set to V_{LSG} = -90.0 mV. We then performed two of these measurement series; once to determine the effect of lead coupling on the emission linewidth, and once to determine the effect of the lead coupling on the dephasing of our system.

4.1 Lever Arm

As mentioned in the previous chapter, in order to study the transport through the DQD, we have several methods at our disposal. If we measure the current flowing between source and drain at a bias V_{bias} = -200 μV, we obtain the FBTs. We thus varied the V_{RPG} and V_{LPG} voltages, thereby adjusting the

quantum dot levels with respect to each other. As long as these levels still sit within the bias window, we see a current.

We can then use the FBTs to extract the lever arm values. The lever arms (α) allow us to convert between gate voltage and energy and will be required in later measurements. They are given by the following expressions:

$$\alpha_1 \delta V_{g1} = |eV|, \qquad \alpha_2 \delta V_{g2} = |eV|, \tag{4.1}$$

where δV_{g1} and δV_{g2} are the dimensions of the FBT as shown in Figure 4.1 [10].

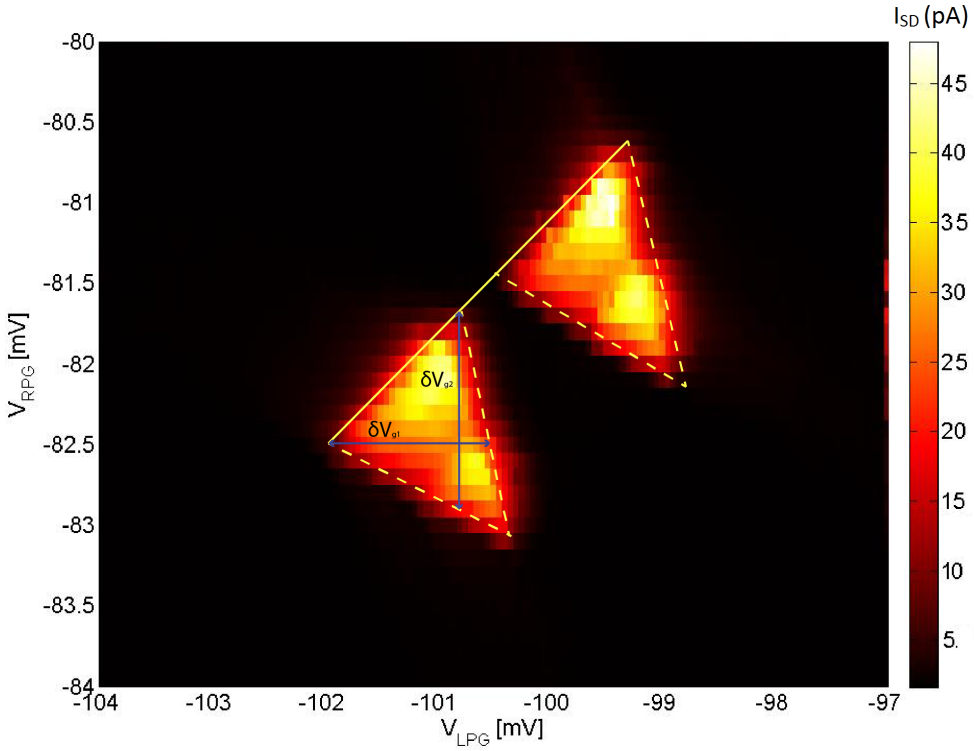

Figure 4.1: A measured set of FBTs. We measured the current between source and drain at a finite bias (V_{bias} = -200 μV) while varying V_{LPG} and V_{RPG}. The relevant dimensions required to obtain the lever arms are indicated with dark blue arrows.

Our initial FBT measurement was performed at $V_{SDB} = -87.5$ mV, $V_C = -20.0$ mV and $V_{RSG} = -14.0$ mV. From here, we can use the equation above to extract lever arm values of

Left Triangle	$\alpha_1 = 0.132$	$\alpha_2 = 0.155$
Right Triangle	$\alpha_1 = 0.116$	$\alpha_2 = 0.160$

We will find later that for fitting purposes it is best to approximate a single value of the lever arm.

4.2 Inter-dot Tunnel Coupling

The second measurement that is critical for analysing the emission data is to determine the inter-dot tunnel coupling. As mentioned, we want to make sure that this particular coupling remains constant. In order to perform this measurement, we apply an RF microwave tone at a frequency ν_r equal to the bare cavity frequency, ν_o, of the resonator. These RF measurements are performed at zero bias meaning that electrons can only tunnel elastically when all energy levels are degenerate, i.e. along the bottom edge of the FBT. At this point, due to the coupling between the DQD and the resonator, a charge shift in the DQD leads to a frequency shift in the RF signal, which manifests itself as a phase shift. This can be explained in terms of a dipole coupling between the dot and resonator [14]. We are able to, through heterodyne detection, determine both the amplitude and phase of the signal.

At each measurement point, we then made such an RF measurement by measuring the phase shift in the resonator while varying V_{LPG} and V_{RPG} as shown in Figure 4.2a. Again, the phase shift only occurs along the bottom

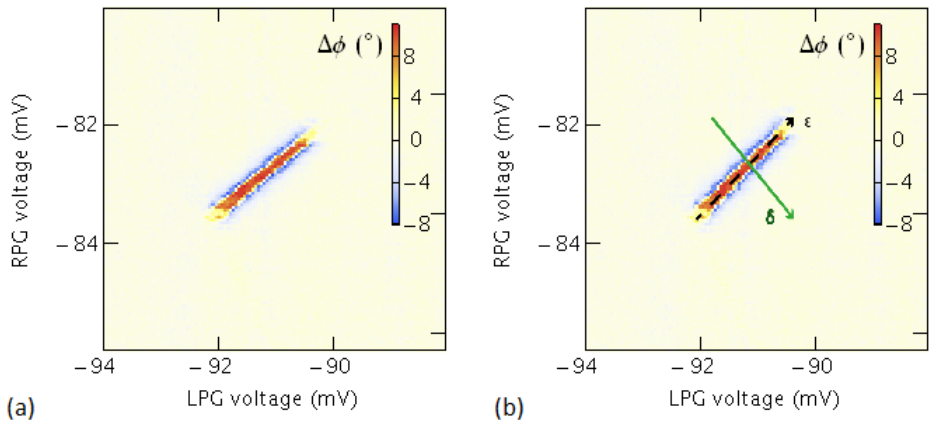

Figure 4.2: The phase shift of the resonator signal obtained through heterodyne detection. (a) We see the phase shift occurs along the line connecting the two FBTs. (b) Along the ϵ axis, the quantum dot levels are varied evenly and remain degenerate. We measure the frequency shift along the δ axis, where the detuning between the dot levels is varied.

edge of the two FBTs, that is, along the line connecting the two triple points, due to the energy level degeneracy. This is known as the energy axis, as the dot levels energies are being adjusted evenly. Ultimately however, we want to measure the frequency shift. This is done by measuring along the detuning axis, perpendicular to the energy axis, as shown in Figure 4.2b.

Along this axis, we change the detuning between the two dot levels, and so expect a frequency shift as we approach zero detuning.

In order to extract the interesting parameters, we need to model this frequency shift. This can be achieved by modelling the coupling between our DQD (two-level system) and resonator (harmonic oscillator) using the Jaynes-Cummings Hamiltonian

$$H = h\nu_o(\hat{n} + \frac{1}{2}) + \frac{h\nu_q}{2}\hat{\sigma_z} + \hbar g \sin\theta(\hat{a}^\dagger\hat{\sigma}^- + \hat{a}\hat{\sigma}^+), \tag{4.2}$$

where $\nu_q = \sqrt{\delta^2 + 4t^2}$ and $\sin\theta = 2t/\sqrt{\delta^2 + 4t^2}$ [14]. Note that ν_o is the bare resonator frequency and g is the resonator-dot coupling. By solving the master equation, one can obtain the steady state of the system, and so model the frequency shift as a function of detuning as shown in Figure 4.3. As part of this model we also need to give the lever arm values. However, in

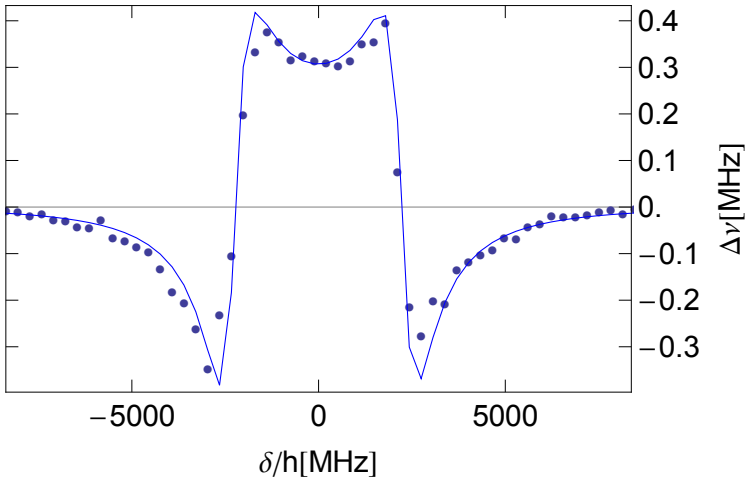

Figure 4.3: We see here the shift in the resonance frequency as a function of the detuning between the quantum dot levels. The dots represent the data, measured along the detuning axis in the center of the phase shift. The solid line is the Jaynes-Cummings model with a coupling $g/2\pi$ =11.5 MHz, dephasing $\gamma_\phi/2\pi$ =100 MHz and inter-dot tunnel coupling $2t/h$ = 6.48 GHz.

this case, we only use a single lever arm, and so, rather than using the value extracted earlier, we use a value producing a satisfactory fit to the data, (α = 0.093). From this model, we can also extract the values for t, g, and γ_ϕ, the dephasing, which lead to good agreement.

By adjusting the value of V_C, we were able also adjust the value of t. This process of measuring and modelling was repeated until the desired inter-dot

tunnel coupling (6.9 GHz for the first series and 6.1 GHz for the second) was obtained.

4.3 Emission Linewidth

The last form of measurement that we performed is to measure the photon signal emitted by the DQD directly. Note that in this case, the RF microwave tone was turned off and a finite bias, V_{bias} = -200 μV, was applied. From the FBT measurements described earlier, we perform a series of measurements along a line passing through the lower triangle, parallel to the detuning axis as shown in Figure 4.4. At each point, corresponding to a different detuning

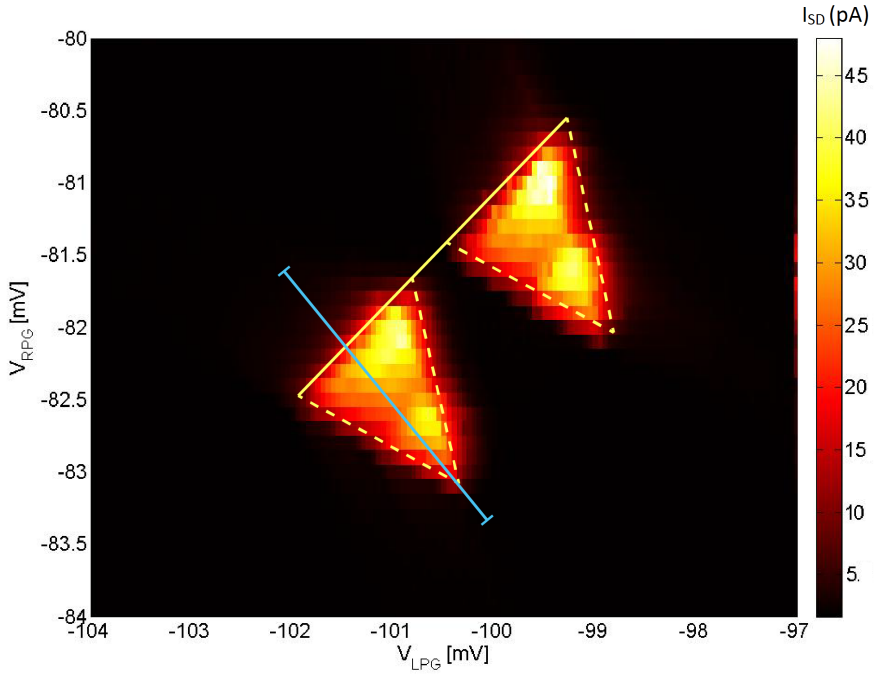

Figure 4.4: A measured set of FBTs as in Figure 4.1. Here, we show the axis along which we perform the FBT measurements in light blue. At each point, we measure an average of 20 PSDs alternating between bias on and bias off.

value, we measure the power spectral density (PSD), which is the Fourier transform of the first-order auto-correlation function [15]

$$S = FT((I + iQ) * (I + iQ)). \tag{4.3}$$

Due to our signal being very small, we use the amplifiers described briefly in Chapter 3. Furthermore, we average over twenty measurements alternating

between a finite bias (corresponding to signal) and zero bias (no signal), which we subtract in order to increase the visibility of the signal.

If we then integrate the PSD, we obtain the emission power as a function of detuning, as shown in Figure 4.5. Note that we see two resonances near each

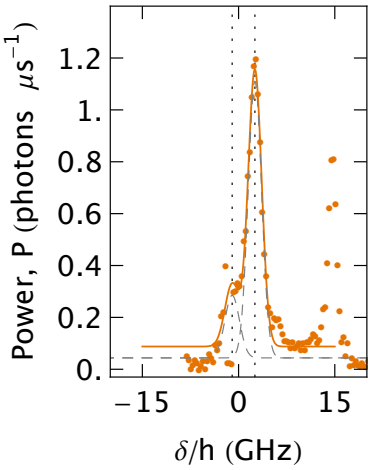

Figure 4.5: An emission power measurement showing the emission power as a function of detuning. We clearly see two peaks centered around zero detuning. These two have been fitted separately using a Gaussian form (in dashed grey), the sum being shown in orange. To the right, at large detunings, we see another peak belonging to an excited state. Note that this measurement was performed at an inter-dot tunnel coupling of $2t/h = 6.65$ GHz.

other and another towards larger detuning values. If we recall, we expect to see an emission signal when the qubit transition frequency $\nu_q = \sqrt{\delta^2 + 4t^2}$ is resonant with the resonator frequency ν_o. Thus, we should see an emission signal at two detunings: $\delta = \pm\sqrt{\nu_o^2 - 4t^2}$, corresponding to forward and reverse detuning respectively. The first two resonances that we see, centered around zero detuning, are exactly these corresponding to the two detunings. Note also that the resonance at negative (reverse) detuning is much smaller, due to the hybridization. The third resonance, towards large detuning is due to an excited state, also seen in Figure 4.4 near the triangle peak.

From these emission power measurements, we can extract the linewidths, giving us the broadening of the quantum dot states. We have two methods at our disposal in order to fit the two resonances. The first possibility is fitting each resonances individually with a Gaussian as shown in Figure 4.6a. The second possibility is to use Equation 2.4 as shown in Figure 4.6b. If we replace $\nu_q = \sqrt{4t^2 + \delta^2}/h$,

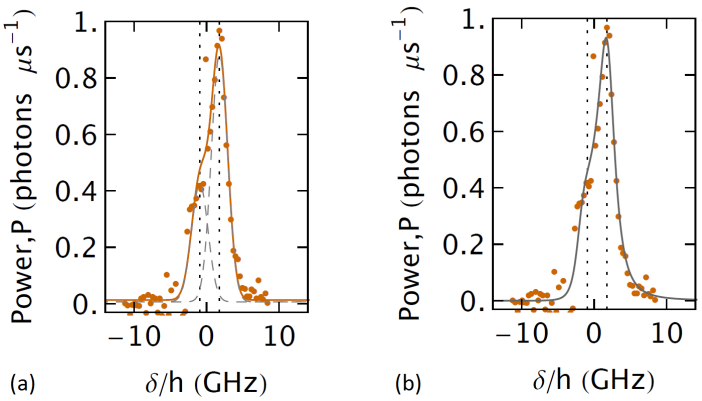

Figure 4.6: An emission power measurement at $2t/h$ =6.92 GHz showing the emission power as a function of detuning. Note that the lead coupling at this point is determined by the current at zero detuning, which is 160 pA in this case. We have fitted the data points using two methods. (a) We fit the resonances individually using a Gaussian. The individual Gaussians are shown in dashed grey and the sum is shown in orange. (b) We fit the two resonances at the same time using Equation 4.4.

$$P(\delta/h) = A(\delta)\frac{\Gamma/2}{(\sqrt{4t^2+\delta^2}/h - \nu_o)^2 + (\Gamma/2)^2}, \tag{4.4}$$

we find that our Lorentzian form is not a true Lorentzian as a function of detuning due to the δ^2 term. Thus, though the linewidth is not given by Γ, it is still closely related, making Γ a very useful parameter. The Gaussian fit on the other hand does give an actual linewidth.

At each point in the measurement series, we first perform an RF measurement to ensure that $2t/h \approx 6.9$ GHz. Then we obtain the emission power and perform the fits to obtain the emission linewidth as a function of the lead coupling. Note that we aren't actually measuring this lead coupling directly. Instead, we consider the current. There are two contributions; elastic and inelastic current. At a zero detuning, around which the emission signal is centered, the elastic current dominates. We can describe it using the following Lorentzian form:

$$I_{el} = \frac{e4(t/h)^2\Gamma_R\Gamma_L}{4(t/h)^2(2\Gamma_L+\Gamma_R) + 4(\delta/h)^2\Gamma_L + \Gamma_L\Gamma_R^2} \tag{4.5}$$

When $t \gg \Gamma_L \approx \Gamma_R$, the current is limited by the tunnelling to and from the leads, not between the dots. In this limiting regime, we find that the current is proportional to the lead coupling. We start off in this regime, and move into one where $t \approx \Gamma_L \approx \Gamma_R$. In this regime, we still find that the proportionality roughly holds. Thus, we can examine how our system behaves as a function of current, which is then effectively its behaviour as a function of lead coupling.

Chapter 5

Results

Having described the various measurement techniques, we can examine the effect of the lead coupling on the dephasing and emission linewidth in more detail.

5.1 Dephasing

As discussed in the previous chapter, we performed a series of measurements at an inter-dot tunnel coupling $2t/h$ of 6.1 GHz. At each successive measurement, we decreased the values of V_{SDB} and V_{RSG}. In doing so, we decreased the tunnel coupling to the leads, and thus, the current. Using the Jaynes-Cummings model, we can examine the behaviour of the dephasing $\gamma_\phi/2\pi$ as a function of current. This is shown in Figure 5.1.

In this Figure, we plot the dephasing as a function of the maximum current observed in the FBT measurement. At each point in this measurement we keep the inter-dot coupling constant at $2t/h$ = 6.1 GHz. For currents above 100 pA, the resonator-dot coupling is given by $g/2\pi$ = 12 GHz and below, $g/2\pi$ = 10 GHz. This yields better agreement between measurement and theory. The physical motivation is as follows. As we decrease V_{SDB}, we expect the surface area of our dot to become smaller, thereby reducing the capacitive coupling.

What we see is that for currents below 500 pA, the lead coupling seems to have very little effect on the dephasing, which varies slightly around $\gamma_\phi/2\pi$ = 150 MHz. At large currents (large lead tunnel couplings), we find that the dephasing increases very quickly. This is likely due to the fact that at such large couplings, the barrier between lead and dot is very small, leading to poorly defined dots, and thus, very large decoherences.

Furthermore, we can also look at the current as a function V_{SDB} as shown in Figure 5.2. The figure shows a log plot of the current as a function of

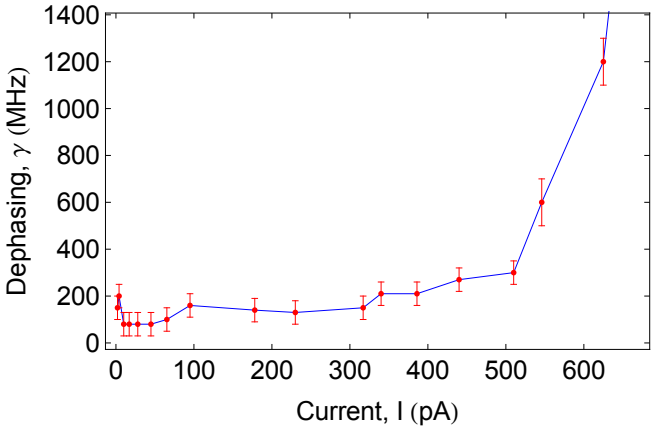

Figure 5.1: Here we see the dephasing γ_ϕ of our system, as obtained from the Jaynes-Cummings model, as a function of the maximum current between source and drain. For currents below 500 pA, the dephasing is varies slightly around 150 MHz. Above this point though, it increases very quickly. The error bars ($\pm$ 50 MHz below 500 pA and $\pm$ 100 MHz above) were determined to be appropriate based on visual agreement between model and data. The blue line acts as a guide to the eye.

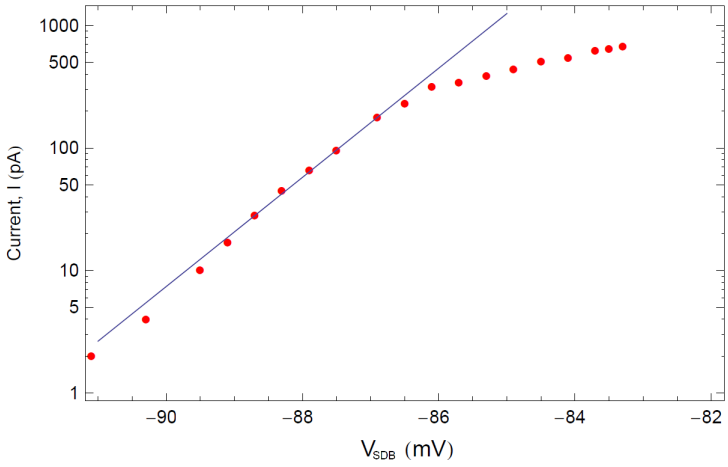

Figure 5.2: This figure shows the current between source and drain on a log scale as a function of V_{SDB}. As V_{SDB} determines the potential barrier height and width, we expect that the current should increase exponentially with the voltage. The red points give the experimental data, and the blue is an exponential fit.

V_{SDB}. As this voltage determines the width and height of the potential barrier that the electrons must tunnel through, we would expect the current to increase exponentially with V_{SDB}. What we see is that (starting with a very negative voltage and increasing towards zero), the current indeed increases exponentially with the voltage up to $V_{SDB} \approx$ -86 mV. At this point, the behavior changes suddenly, and while it appears to be exponential again,

it has very different parameters. The reason for this is unclear, but it could be that the gate response isn't quite what we expect.

5.2 Emission Linewidth

Finally, we want to examine how the emission linewidth described in Section 4 changes with respect to the lead coupling, as evidenced by its behaviour as a function of current. As mentioned, we performed a series of PSD measurements at a constant inter-dot tunnel coupling of $2t/h \approx 6.9$ GHz and integrated to get the emission signal. Note that the inter-dot tunnel coupling was measured at zero bias, as shown in Figure 4.2. However, at the point at which we measure, and due to applying the bias while measuring the emission linewidth, the actual inter-dot tunnel coupling shifts slightly to smaller values. However, as we remain consistent in these measurements, the coupling should be still be the same between all the measurements.

Using the Gaussian fit, we fitted the two peaks centered around zero detuning separately and plotted the value of the FWHM of the Gaussian as a function of the current at zero detuning. Similarly, we used the Lorentzian fit to obtain a value for Γ, and we also plotted Γ as a function of the current at zero detuning. These plots are shown in Figure 5.3. Thus, each point in this figure corresponds to a curve fit as shown in Figure 4.6

Here, we can see very clearly that the linewidth, as given by the FWHM of the Gaussian fits, as well as the value of Γ, which is related to the linewidth, are proportional to current. For small currents we were somewhat limited in our ability to resolve the two peaks, making the fitting very difficult. Nonetheless, the trend is very clear, and thus, increased current, corresponding to increased lead coupling, leads to increased qubit level broadening.

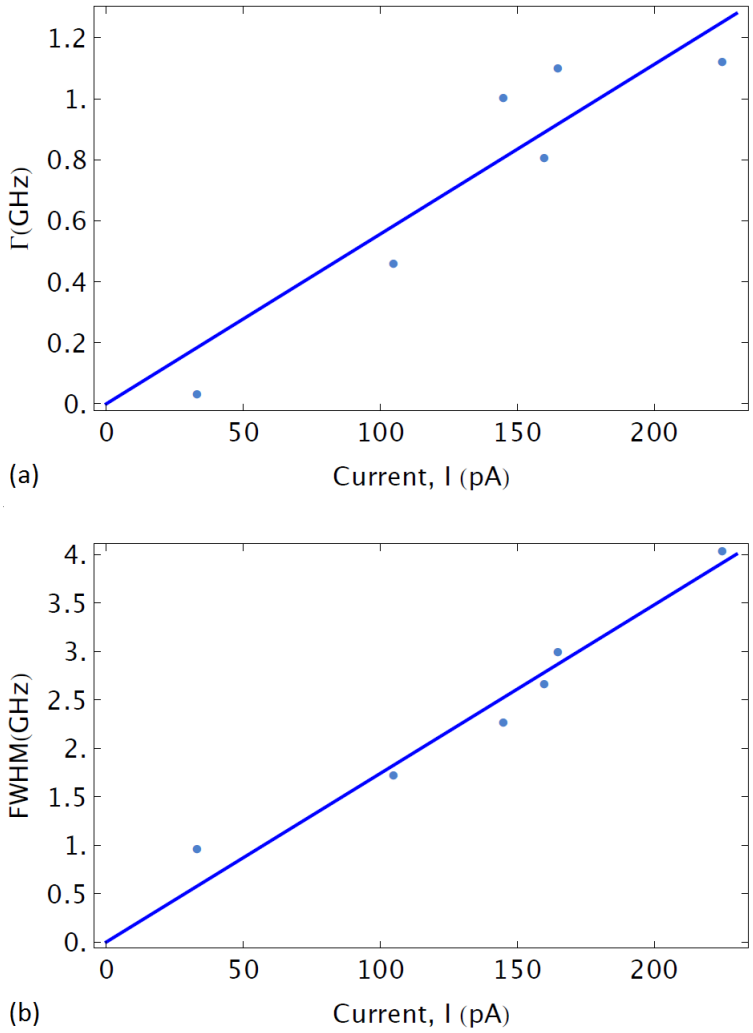

Figure 5.3: Here we see the results of the emission power peak fits. We plot the quantum dot broadening in terms of (a) the Lorentzian Γ and (b) The Gaussian FWHM as a function of the current. The light blue points are the fits obtained for various V_{SDB} and V_{RSG} configurations. The linear fit, given by the dark blue line, is forced through 0.

Chapter 6

Summary

In this thesis, we have discussed gate-defined double quantum dots both in terms of structure, as well as transport properties. This transport was discussed both in the absence and presence of a bias between source and drain. We saw that for zero bias, we expect transport only when all energy states are degenerate, whereas at a finite bias, we observe finite-bias triangles; triangular regions of electron transport. We discussed both elastic and inelastic tunnelling, and how inelastic tunnelling leads to an emission signal from which we can extract the width of the quantum dot energy levels.

Furthermore, we examined the various methods, DC, RF microwave and emission signal, which we can use to quantify some aspect of the single-electron transport. From these measurements, we showed how we can extract the lever arm, inter-dot tunnel coupling, dephasing and emission linewidth. We continued by examining the effect the coupling to the leads has on the dephasing and emission linewidth by varying V_{SDB} and V_{RSG} while maintaining a constant inter-dot tunnel coupling.

What we found was that the dephasing is independent of the coupling to the leads up to a coupling corresponding to a current of approximately 500 pA, where the dots seem to be ill-defined. We assume that the lead coupling varies exponentially with V_{SDB}. However, at $V_{SDB} \approx$ -86 mV, there is a change in the exponential behaviour, indicating that this assumption may only be true up to a certain point. Nonetheless, in this regime, the current should still be proportional to the lead coupling. Finally, we measured the emission linewidth using both Gaussian and Lorentzian fits, and found that the quantum dot broadening increases linearly with current. That is, the quantum dot linewidth is proportional to the coupling to the source and drain.

Bibliography

[1] A. Wallraff, D. I. Schuster, A. Blais, L. Frunzio, R.S.Huang, J. Majer, S. Kumar, S. M. Girvin, and R.J.Schoelkopf, Nature (London) **431**, 162 (2004).

[2] R. J. Schoelkopf and S. M. Girvin, Nature (London) **451**, 664 (2008).

[3] A. Blais, R.S. Huang, A. Wallraff, S. M. Girvin, and R. J. Schoelkopf, Phys. Rev. A **69**, 062320 (2004).

[4] I. Thomas. Semiconductor Nanostructures,Oxford University Press, New York, NY (2010).

[5] O. Zilberberg, B. Braunecker, D. Loss. Phys. Rev. A **77**, 012327 (2008).

[6] H.R. Wei, F.G. Deng, arXiv:1206.0202.

[7] See Supplemental material for [9].

[8] V.N. Stavrou, X. Hu, Phys. Rev. B **72**, 075362 (2005).

[9] A. Stockklauser, V.F. Maisi, J. Basset, K. Cujia, C. Reichl, W. Wegscheider, T.Ihn, A. Wallraff, K. Ensslin. Phys. Rev. Lett. **115**, 046802 (2015).

[10] W.G. van der Wiel, S. De Franceschi, J.M. Elzerman, T. Fujisawa, S. Tarucha, L.P. Kouwenhoven. Rev. of Mod. Phys. **75**, 1 (2003).

[11] T. Fujisawa, T.H. Oosterkamp, W.G. van der Wiel, B.W. Broer, R. Aguado, S. Tarucha, L.P. Kouwenhoven. Science. **282**, 5390 (1998).

[12] T. Fujisawa, W.G. van der Wiel, L.P. Kouwenhoven. Physica E **413-419**, 7 (2000).

[13] A. Stockklauser, Ensslin Group Meeting, ETHZ, 09.10.2015.

[14] T.Frey, P.J. Leek, M. Beck, A. Blais, T.Ihn, K. Ensslin, A.Wallraff. Phys. Rev. Lett. **108**, 046807 (2012).

[15] C. Lang, D. Bozyigit, C. Eichler, L. Steffen, J. M. Fink, A. A. Abdumalikov Jr., M. Baur, S. Filipp, M. P. da Silva, A. Blais, and A. Wallraff, Phys. Rev. Lett. **106**, 243601 (2011).

ETH

Eidgenössische Technische Hochschule Zürich
Swiss Federal Institute of Technology Zurich

Declaration of originality

The signed declaration of originality is a component of every semester paper, Bachelor's thesis, Master's thesis and any other degree paper undertaken during the course of studies, including the respective electronic versions.

Lecturers may also require a declaration of originality for other written papers compiled for their courses.

I hereby confirm that I am the sole author of the written work here enclosed and that I have compiled it in my own words. Parts excepted are corrections of form and content by the supervisor.

Title of work (in block letters):

LEAD COUPLING EFFECTS IN DOUBLE QUANTUM DOTS.

Authored by (in block letters):

For papers written by groups the names of all authors are required.

Name(s):	**First name(s):**
HEDRICH	NATASCHA.

With my signature I confirm that

- I have committed none of the forms of plagiarism described in the 'Citation etiquette' information sheet.
- I have documented all methods, data and processes truthfully.
- I have not manipulated any data.
- I have mentioned all persons who were significant facilitators of the work.

I am aware that the work may be screened electronically for plagiarism.

Place, date	**Signature(s)**
ETHZ Hönggerberg,	

For papers written by groups the names of all authors are required. Their signatures collectively guarantee the entire content of the written paper.